Scalable Computing: Practice and Experience, ISSN 1895-1767, http://www.scpe.org
© 2024 SCPE. Volume 25, Issues 4, pp. 2795–2808, DOI 10.12694/scpe.v25i4.2821

THE APPLICATION CHARACTERISTICS AND CREATION OF DIGITAL SCULPTURE BASED ON PARAMETER MODEL

ZHAO XU* AND QIUYANG LI†

Abstract. Recently, digital sculpture based on parametric models has emerged both domestically and internationally; To improve the accuracy and efficiency of constructing digital sculpture parameter models, this study proposes a method for constructing digital sculpture parameter models based on improved point cloud registration algorithms by iterating the nearest point algorithm and multi-scale matrix descriptors to increase the iteration efficiency and accuracy of point cloud registration algorithms. The results show that under the Bunny model, the number of three scale feature points is 2146, and the coarse registration error is 0.925 * 10-6 m; As the noise increases, the efficiency of the algorithm proposed in the study increases by an average of 10.1%; The average relative rotation error is reduced by 1-2 orders of magnitude, and the registration time is shortened by 62.7% on average; For a 30dB noise point cloud, it is reduced by one order of magnitude, and as the noise increases, the efficiency of the algorithm proposed in the study increases by an average of 10.1%. In the Dragon model, the number of three scale feature points is 2235, the coarse registration time is only 26 seconds, and the registration error is 0.285 * 10-5m; The average relative rotation error is reduced by 1-2 orders of magnitude, and the registration time is shortened by 62.7% on average. The digital sculpture creation method on the ground of parameter models proposed in this study has improved the registration accuracy and efficiency of parameter models.

Key words: Digital sculpture; Point cloud registration; Parameter model; Application characteristics; Iteration closest point

1. Introduction. Digital sculpture (DS) embodies a high degree of integration between science and art, giving artistic forms a rational mathematical order. DS refers to the use of computer technology and information technology to digitize traditional sculpture and apply it to the field of sculpture. DS can be divided into two types: parametric model-based DS and physical model-based DS. Parametric modeling-based DS refers to the creation of a three-dimensional digital model through parametric modeling and its application in DS creation. Compared to the first two, DSs on the ground of physical models can better represent the true form of materials, but the production efficiency is lower and the production cost is higher [3]. From a technical perspective, parameter modeling is the application of digital casting and rapid prototyping manufacturing technology in traditional handicrafts. This technology can shorten the traditional product design and production cycle from months to days or even minutes, with the ultimate goal of providing designers with a better user experience [4, 5]. The existing algorithm selects reference points from the front surface of the input model, and the modeling result is prone to unreasonable height level phenomenon. To solve the defects such as cusps, another height field reconstruction is required, which multiplies the amount of numerical computation and results in low modeling efficiency. Moreover, the existing algorithm can only conduct digital sculpture modeling for 3D mesh models with a single topology, and cannot process 3D models with complex topology structures, otherwise topological tearing will occur after model deformation. The existing algorithm can only deal with the triangular mesh model of manifold, and can not deal with the triangular mesh model with sharp edge. If the model containing non-manifold triangular mesh is used for modeling, the program will crash and so on. Compared with triangular grid data, point cloud data has the advantages of simple representation and convenient acquisition. The modeling method based on point cloud deep learning can get rid of the shackles of grid model and make modeling more flexible. In order to solve the above problems, the mesh modeling method based on differential deformation theory can effectively deal with complex topological structure problems, while the point cloud modeling method based on iterative nearest point improvement can get rid of the bondage of the mesh model and make the

*College of Art and Design, Heilongjiang Institute of Technology, Harbin, 150050, China.
†College of Art and Design, Heilongjiang Institute of Technology, Harbin, 150050, China (liqiuyang8721@163.com)

modeling more flexible. The research of this paper will promote the degree of automation of digital sculpture design to a certain extent, reduce the intensity of digital sculpture design, and provide a theoretical basis for subsequent research.

The article conducts research through four. The first is a review of the current research status of DS and parameter model construction methods; The second is the application feature analysis of DS and the construction of a DS parameter model on the ground of an improved point cloud registration algorithm; The third is to verify the performance of the parameter model designed in the research; The fourth is the conclusion.

2. Related works. The emergence and development of parameter modeling technology are mainly influenced by computer technology and information technology, and its application fields have also expanded from traditional sculpture to fields such as film and television special effects and virtual reality. Sun et al. proposed a lumped parameter model for liquid sloshing in a rigid cylindrical groove with multiple rigid partitions to improve the accuracy of dynamic analysis of complex fluid solid systems and reduce computational workload; By dividing the fluid domain into simple subdomains, the value of the convective velocity potential is obtained, and the equivalent lumped parameter model is established according to the same shear and torque generated with the Analytical expression; After verification, the model has feasibility [6]. Zhou and other scholars proposed an improved model on the ground of hybrid adaptive Particle swarm optimization hybrid Simulated annealing algorithm to solve the problem of poor accuracy and robustness of traditional battery parameter models; This model used three equivalent circuit models to conduct experiments on three different types of batteries, and its accuracy and adaptability were tested; The results show that the parameter model has a fast Rate of convergence and accurate prediction ability [7]. The Sequeira team has established a high computational efficiency and accuracy motor parameter model to improve the thermal management of the motor; This model verifies the lumped parameter thermal network of the motor through commercial motor CAD modeling, and conducts detailed finite element analysis, taking into account all key parameters; The final results indicate that the contact resistance sensitivity between the lining and the lamination is high, and the maximum temperature difference between the slot winding and the end winding is 2% [8]. Qin et al. proposed cascade visual geometry coding, which can improve point cloud registration through the visual information of RGB images. Intermodal features are iteratively fused by using the inductive bias of 2D and 3D convolution to better consider the correlation between the two modes. Geometry-centric coding modules first use three-dimensional convolution in geometric space to enhance visual features, thereby explicitly embedding geometric information, and enhance the salience and relevance of local features through two-dimensional convolution [9]. Zhang et al. innovatively introduced face template deformation into portrait relief modeling, matched key points on the image with feature points on the template, and made the face template fit the target face on the image by minimizing the distance between the two. To solve the problem of missing height field detail after feature matching, the illumination parameters are obtained by solving a linear system containing the intensity of image pixels and the normal information of model vertices. SFS is used to optimize the height field of the face model. Finally, the linear compression of height field and Laplasian detail enhancement techniques are used to generate high relief of face [10].

After decades of development, DS has become increasingly mature in technology and its application scope has also been expanding. In addition to its application in the field of sculpture, DS has also expanded to other fields, and more and more artists and designers have conducted research and exploration on it. Edward et al. proposed a generation algorithm for the axial generation process; This algorithm creates various types of DSs by calculating color values and dynamically increasing the size of shapes; Compared with methods on the ground of manipulating pixels/voxels and tracking particle paths, this method has good balance performance and the ability to create complex visual effects [11]. The Zhou team introduced an automated system to design a vivid brick sculpture to represent a three-dimensional model; This system transforms the building model into a LEGO sculpture while maintaining its original styling characteristics. By extracting the visual features of the model, various transformation parameters are obtained; Then it used a deformation algorithm to eliminate the differences between discrete positions, ultimately generating a vivid LEGO DS [12]. Liu et al. proposed a 3D visual measurement method on the ground of digital image processing to improve the noise resistance of 3D measurement systems; This method eliminates most of the environmental noise by designing the optimal weight function. Under the spatio-temporal background of the video sequence, the decision Tree model is used to extract and track the stripes; The results indicate that in complex lighting environments, this method

can accurately measure in real-time, providing support for DS modeling [13]. Ramazan and other scholars proposed an automatic key point detection and matching method on the ground of iterative nearest point algorithm before rough registration of point clouds to improve the precision of fine registration of DS; This method matches the model through the geometric relationship between key points and the angle and distance between key points; The results show that the algorithm has higher accuracy and fewer iterations [14]. Lanteri et al. proposed a new digital photogrammetry method using Agi soft Photos can® software to better define the drawing details of DS; This method highlights the detailed features of the model through the generated UV 3D model, and restores the vivid expression of the model through the infrared 3D model; This method has the advantages of non-invasive, economical, and efficient [15].

In summary, although researchers have proposed many methods for constructing DS parameter models on the ground of different algorithms and have achieved certain results, they lack accuracy, robustness, and efficiency; Therefore, through the improved point cloud registration algorithm-based DS parameter model, it is expected to be able to quickly and accurately achieve the creation of DS.

3. Research on the Application Characteristics and Parameter Model Construction of Digital Sculpture. This study designed a DS creation method on the ground of parameter models through an improved point cloud registration algorithm; This method first obtains the Multi scale Matrix Descriptor (MSM) by optimizing the curvature change, measuring angle and eigenvalue property (CME), then detects the key points using the Local Surface Patches (LSP) algorithm, and finally corrects them using the Iterative Closest Point (ICP) algorithm.

3.1. Analysis of the Application Characteristics of Digital Sculpture. The creation of traditional sculpture is a "linear" production process. For example, clay sculpture is the process of first setting up a frame, then laying large pieces of mud, and finally thoroughly shaping the form. This process is irreversible, that is, the order of each step cannot be arbitrarily changed, let alone jump to one of the steps. The problem with the "linear" method is that when an error occurs in the first step, to correct the error, one must step back and start over. Compared with traditional sculpture, DS has significant differences in the creative process. These differences come from the characteristics of computer technology on the one hand, and the differences in the properties of materials themselves on the other hand [16]. Using modeling software to create sculptures, the materials used will not be real soil, stone, wood, or metal, but rather computer data.

DS has deep "interactivity" characteristics, while traditional sculpture works often exhibit "non interactivity". In traditional sculpture art, it takes a lot of time to carve a standard cube or sphere from a statue. In DS systems, real-time observation and feedback of sculpture effects are achieved by simply processing sculpture data through command tools [17, 18]. For example, by using modeling software, a standard sphere can be peeled off from the sculpture in the shortest possible time and the effect can be seen quickly. The most essential feature of DS is its virtualization and digitization, which is not affected by natural forces and can simulate the effects of natural forces. Its shape is easy to penetrate, can be quickly replicated, and does not occupy physical space. DS has broken the limitations of sculpture in space, while also causing changes in the preservation and shaping of artworks.

Point cloud registration algorithm modeling is one of the creative methods for many DS. The point cloud registration algorithm collects data from multiple locations, which can be used to represent differences in objects, terrain, or other details in a certain area. The parameter model construction process using point cloud registration algorithm is shown in Figure 3.1. Firstly, it inputs the source point cloud and the target point cloud, and then comprehensively considers factors such as curvature change, measurement angle, feature values, etc. to obtain CME; By optimizing the normal vector angle, point density, curvature, and other factors of the three scale feature points, the MSM is obtained; Then the matching relationship is initially established, and the unit Quaternion algorithm is used to calculate the initial registration parameters to achieve rough registration. Finally, the ICP algorithm was modified to achieve ICP registration.

The curvature reflects the degree of deviation of the surface from the plane. For a given point p_i , the more intense the depth change of the neighborhood, the more obvious the areal feature centered on point p_i. The

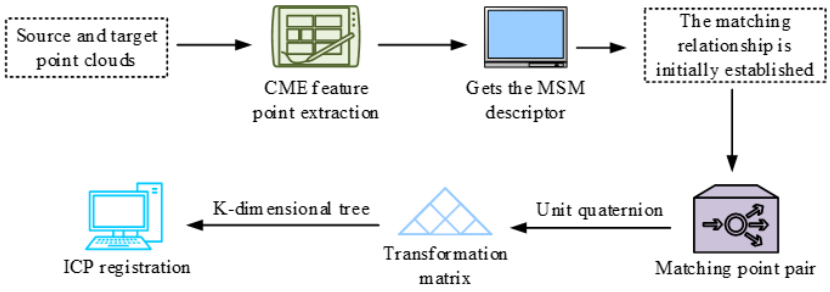

Fig. 3.1: Flowchart of parameter model construction

weighted covariance matrix of point p_i in the neighborhood with radius r is shown in equation 3.1.

$$\begin{cases} Cov(p_i) = \frac{\sum_{|p_i-p_j|\leq r} \omega_{ij}(p_i-p_j)(p_i-p_j)^T}{\sum_{|p_i-p_j|\leq r} \omega_{ij}} \\ \omega_{ij} = \frac{1}{|p_i-p_j|} \end{cases} \tag{3.1}$$

In equation 3.1, p_j is the neighborhood point. This study sets P as a point cloud, consisting of N points, given a query point $p_i \quad (i \in [1, N])$; Its neighborhood is a sphere with a center of p_i and a radius of r. The adjacent points of p_i on the sphere are represented by p_{ik} , and k is the number of adjacent points of p_i . The Covariance matrix in the sphere is constructed by taking $\bar{p}_i$ as the center of mass of p_{ik}. The specific formula is shown in Equation 3.2.

$$\mathrm{Cov}_2(\mathbf{p}_i) = \begin{bmatrix} \mathbf{p}_{i1} - \bar{\mathbf{p}}_i \\ \vdots \\ \mathbf{p}_{ik} - \bar{\mathbf{p}}_i \end{bmatrix}^T \begin{bmatrix} \mathbf{p}_{i1} - \bar{\mathbf{p}}_i \\ \vdots \\ \mathbf{p}_{ik} - \bar{\mathbf{p}}_i \end{bmatrix} \tag{3.2}$$

The cos values of the two normal vectors p_i and p_{ik} are used as the first scale to characterize the fluctuation changes of the point cloud surface area. The calculation method is shown in equation 3.3.

$$F_1(p_{ik}) = \frac{\mathbf{v}_i \cdot \mathbf{v}_{ik}}{|\mathbf{v}_i| \cdot |\mathbf{v}_{ik}|} \tag{3.3}$$

In equation 3.3, $F_1(p_{ik})$ represents the cos values of v_i and v_{ik} ; v_i and v_{ik} represents the normal vectors of query point p_i and adjacent point p_{ik}, respectively; $|v_i|$ and $|v_{ik}|$ represent the modulus of a vector. Then it projects the point set p_{ik} onto a tangent plane perpendicular to v_i, and the Euclidean distance between the projected point and p_i is used as the second scale to describe the point density. The calculation formula is shown in equation 3.4.

$$F_2(p_{ik}) = \sqrt{\|\mathbf{p}_i - \mathbf{p}_{ik}\|^2 - (v_i \cdot (\mathbf{p}_i - \mathbf{p}_{ik}))^2} \tag{3.4}$$

In equation 3.4, $\|\mathbf{p}_i - \mathbf{p}_{ik}\|$ represents the Euclidean distance between two points. The surface curvature, as the third scale, is calculated using Equation 3.5.

$$F_3(p_{ik}) = \frac{\lambda_{i2}}{\lambda_{i0} + \lambda_{i1} + \lambda_{i2}} \tag{3.5}$$

In equation 3.5, $\lambda_{i0} \leq \lambda_{i1} \leq \lambda_{i2}$ is the characteristic value. It combines the histogram matrices of the three scales mentioned above to obtain the MSM descriptor of the feature points. The calculation formula is shown in equation 3.6.

$$M_{\mathrm{MSM}} = \sum_{i=1}^{N} \sum_{k=1}^{j} \left(\mathrm{vote} \left\langle \left| \frac{25F_1(p_{ik})}{2} \right| \right\rangle + \mathrm{vote} \left\langle \left| \frac{15F_2(p_{ik})}{r} \right| + 25 \right\rangle + \mathrm{vote} \left\langle \left| \frac{20F_3(p_{ik})}{\sum F_3(p_{ik})} \right| \right\rangle + 40 \right) \tag{3.6}$$

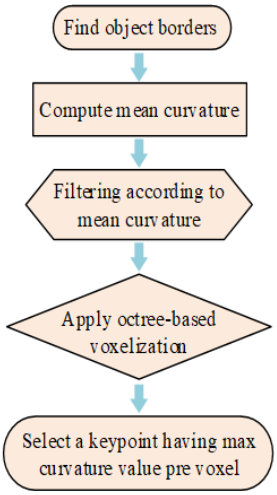

Fig. 3.2: Flowchart of key point detection steps

In equation 3.6, M_{MSM} is an $Nx60$-dimensional matrix; N is the number of feature points; j is the number of neighborhood points; *vote(x)* is a defined function that represents the xth histogram as 1, and $\overline{\sum F_3(p_{ik})}$ is the average value of curvature. Then it establishes a -dimensional tree, searches for the sub vectors with the smallest Euclidean distance between $F(P_m)$ and $F(Q_m)$, and establishes a preliminary matching relationship on the ground of the points corresponding to the vectors; The mathematical expression is shown in equation 3.7.

$$K = \{(h_i^1, h_i^2) \mid h_i^1 \in P_m, h_i^2 \in Q_m, i = 1, 2, \ldots, N_i\} \tag{3.7}$$

In equation 3.7, P_m and Q_m represent the point set for extracting feature points; $F(P_m)$ and $F(Q_m)$ represents the multi-scale matrix descriptors of two point clouds, respectively. Finally, the research uses the unit quaternion algorithm for matching point pair K to calculate the initial registration parameters, namely, rotation matrix R and translation vector T .

3.2. Construction of Digital Sculpture Parameter Model on the Ground of Improved Point Cloud Registration Algorithm. To accurately estimate transformation parameters and improve registration accuracy, strict detection and matching of key points are particularly important [19, 20]. This study selected the LSP algorithm for key point detection, which is a point-by-point significance measurement method. The key point detection steps are shown in Figure 3.2. For the surface curvature of each point, the study used covariance analysis, which utilizes the ratio of the minimum value of each point to the sum of the feature values. However, working directly on the point cloud without any intermediate subdivision, the detector mainly targets samples in high curvature areas, while considering local variation and estimation of second-order error measures. In this method, the maximum surface curvature is considered and voxel-based filtering is applied to improve computational efficiency.

The shape index is introduced here to represent the saliency of vertices, and the specific calculation method is shown in equation 3.8.

$$SI(p) = \frac{1}{2} - \frac{1}{\pi} tan^{-1} \frac{C_{max}(p) + C_{min}(p)}{C_{max}(p) - C_{max}(p)} \tag{3.8}$$

In equation 3.8, *SI(p)* represents the shape index; C_{max} represents the maximum curvature; C_{min} represents the minimum curvature; (p) represents the set of points p. The calculation method for the average shape index

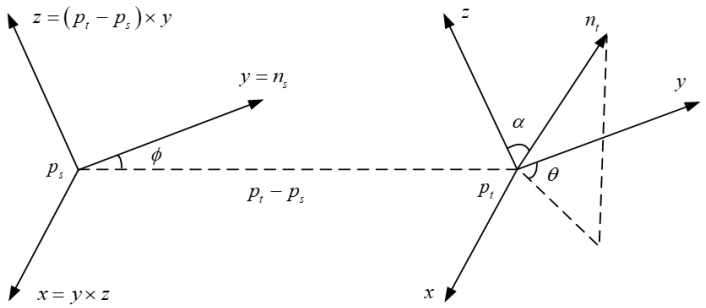

Fig. 3.3: Darboux coordinate system

is shown in equation 3.9.

$$\mu\mathrm{SI}(p)=\frac{1}{N}\sum_{p}\mathrm{SI}(p) \tag{3.9}$$

In equation 3.9, $\mu SI(p)$ is the average shape index; N is the number of points in set (p) . When the SI of a feature point satisfies $\mathrm{SI}(p)\geq(1+\alpha)\mu\mathrm{SI}(p)\vee\mathrm{SI}(p)\leq(1-\beta)\mu\mathrm{SI}(p)$, it can be considered significant, where α and β are scalar parameters. On the ground of this, point cloud points are divided into three-dimensional blocks on the xyz plane, and an appropriate block size dataset is determined on the ground of resolution.

This study utilizes a 3D detector to extract key points from point cloud data, and then uses a 3D descriptor to characterize the neighborhood of the key points and map them to an appropriate space. Ultimately, it is defined as descriptors on different surfaces that match each other. In this method, a 3D keypoint descriptor is a description of the environment around a point in the cloud, but this description is often on the ground of geometric relationships. For two point clouds with similar features, most of the points correspond to the same surface points.

Point feature histogram (PFH) is a common descriptor tool. In addition to point matching, PFH descriptors are also used to identify points in the point cloud, such as edges, corners, and points on the surface. This algorithm adopts a Darboux coordinate system, which is constructed between all pairs of points in the local neighborhood of a point, as shown in Figure 3.3. In the Darboux coordinate system, the source point is a point with a smaller angle between the connecting line of points p_s and p_t and the surface normal. If n_s/t is the normal vector of the corresponding point, then equation 3.10 can be used to represent the structure of the Darboux coordinate system x , y , and z .

$$\begin{cases} x & = y\times z \\ y & = n_s \\ z & = y\times\frac{p_t-p_s}{\|p_t-p_s\|} \end{cases} \tag{3.10}$$

In addition to two normal vectors, the PFH method also uses three angles and one distance element to describe the geometric relationship of point pairs. It adds the four elements of angle and distance to the histogram of point p and the average percentage of point pairs in the p neighborhood, with a similar relationship. In PFH, these histograms are calculated for all possible point pairs in the k neighborhoods of point p . The three angles in the Darboux coordinate system can be represented by equation 3.11.

$$\begin{cases} \alpha & = z\times n_t \\ \phi & = y(p_t-p_s)/\|p_t-p_s\| \\ \theta & = \arctan(xn_t, yn_t) \end{cases} \tag{3.11}$$

This study selected the Iterative Closest Point (ICP) algorithm, which is a point set to point registration method that does not require segmentation and feature extraction of the processed point set to achieve very accurate registration results. Under good initial values, it can also achieve good algorithm convergence. This study sets the target point cloud $P = \{p_i\}_{i=1}^{N_p}$ and the source point cloud $Q = \{q_i\}_{i=1}^{N_Q}$, and each point q_i in the source point cloud Q can be expressed as equation 3.12.

$$q_i' = Rq_i + T \tag{3.12}$$

In equation 3.12, R represents Rotation matrix; T represents the translation matrix. Then, for each point p_i on the target point cloud P , It takes the point p_i and q_i' closest to Euclidean distance as the corresponding point, and obtains the calculation equation 3.13.

$$E(R,T) = \frac{1}{k}\sum_{i=1}^{k}\|Rq_i + T - p_i\|^2 \tag{3.13}$$

In equation 3.13, $E(R,T)$ represents the mean value of the sum of the squares of the residuals, which is defined as the iterative Error function; k represents the number of nearest point pairs. ICP algorithm is to find the minimum value of function 3.13, so as to continuously update the Rotation matrix R and translation matrix T until the cut-off conditions are met. To reduce the iteration time of the ICP algorithm, the study introduced the bidirectional k-dimensional tree ICP algorithm, and on the ground of this, redefined the weight Psi_i of the i-th corresponding relationship; The specific calculation formula is shown in equation 3.14.

$$\Psi_i = \left(1 - \frac{d(p_i, q_i)}{\max d(p_j, q_j)}\right)^2 \tag{3.14}$$

In equation 3.14, $d(p_i, q_i)$ is the distance between two points; $maxd(p_j, q_j)$ is the maximum distance among these corresponding relationships. The larger the distance between points, the lower the weight of the corresponding relationship; A new iterative Error function can be obtained according to equation 3.14, and the specific calculation method is shown in equation 3.15.

$$E'(R,T) = \frac{1}{k}\sum_{i=1}^{k}\Psi_i\|Rq_i + T - p_i\|^2 \tag{3.15}$$

4. Performance analysis of parameter models. This study was conducted on a computer configured with an Intel core i7 2.3GHz CPU and 8GB of memory, running software Matlab 2019a, and using Stanford University's Bunny (35947) and Dragon (56053) point cloud models [14]. By comparing the proposed algorithm with other algorithms, the advantages and disadvantages of registration time and accuracy were analyzed, and the feature point extraction results and registration effects were analyzed.

4.1. Result and Analysis of Feature Point Extraction. Relative rotation error is often used in image processing and computer vision to evaluate the performance of image alignment, registration or attitude estimation algorithms. Relative rotation error measures the difference between the actual rotation Angle and the estimated rotation Angle. The smaller the index, the smaller the difference between the actual measurement and the estimated rotation Angle, the better the performance of the algorithm. The registration time is used to describe the computational resources and time complexity required by the algorithm. The smaller the index, the less time it takes for the digital sculpture to complete the point cloud registration, and the lower the requirements for the equipment. The Stanford dataset is scanned with the Cyberware 3030 MS scanner at Stanford University's Computer Graphics Lab. The scenes in this dataset are generated by the model through random rigid body transformation and the addition of three scales of Gaussian noise. The real point cloud data obtained from various 3D scanning devices mainly uses the point matching relationship between the point clouds to estimate the spatial transformation relationship between the point cloud sequences from different viewing angles, so as to complete the attitude normalization to obtain the point cloud in a larger field of view or carry out three-dimensional reconstruction. The presence of noise in the Stanford data set will disturb the

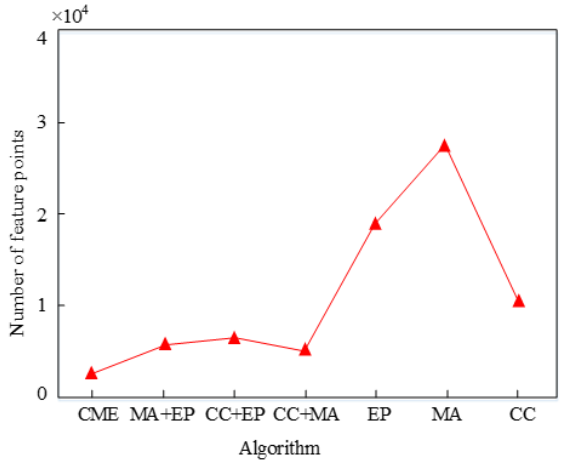

(a) Comparison of the number of feature points

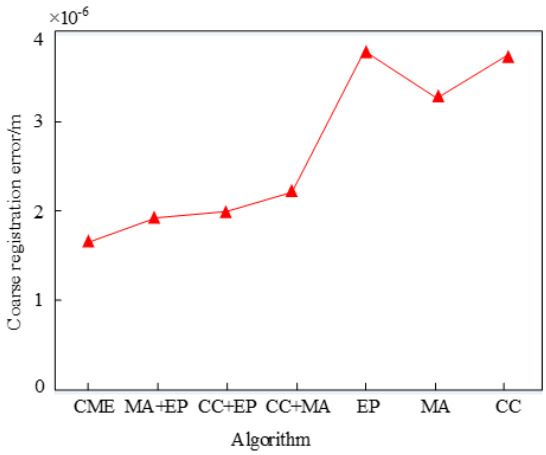

(b) Comparison of Coarse Registration Errors

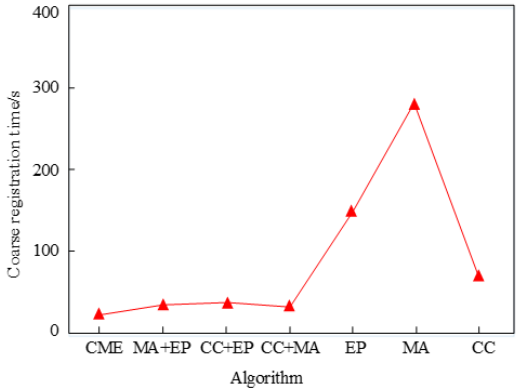

(c) Coarse Registration Time Comparison

Fig. 4.1: Coarse registration results on the ground of Dragon model

local geometry of the point cloud and interfere with the accurate expression of features. Testing in the data set can reflect the registration accuracy of the proposed method. From the real point cloud data set obtained by various 3D scanning devices, the point cloud feature matching method proposed in this paper can solve the three-dimensional rotation and spatial displacement changes generated by the object in a given time, so as to obtain the motion information of the object in three-dimensional space, including velocity and angular velocity, and track the moving object.

To verify the coarse registration performance of feature points in parameter models, this study compared the CME constraint extraction feature points with curvature change (CC), measurement angle (MA), Eigenvalue property (EP), and pairwise combination methods. Figure 4.1 is a comparison of feature point registration on the ground of the Dragon model; Figure 4.1a shows that the number of feature points in a single feature extraction method is much greater than that in a combination method, with MA having the most feature points at 28836 and CME having the least feature points at 2235. Figure 4.1b shows that the coarse registration error of CME is 1.743 * 10-6 m, which is the smallest among several methods, indicating that CME has the best feature point extraction effect. Figure 4.1c shows that MA has the longest coarse registration time, reaching 352 seconds, while CME only has a coarse registration time of 26 seconds.

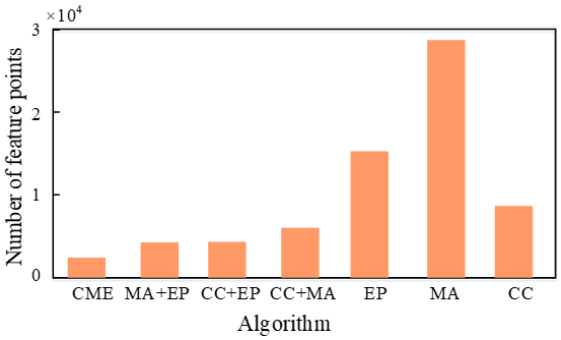

(a) Comparison of the Number of Feature Points

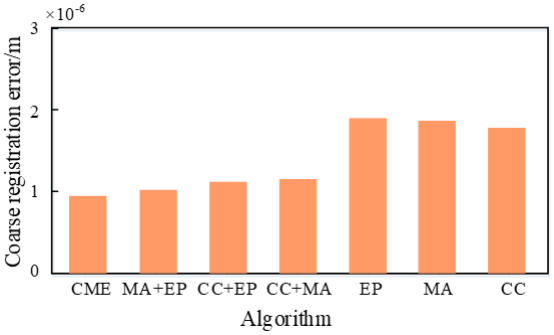

(b) Comparison of Coarse Registration Error

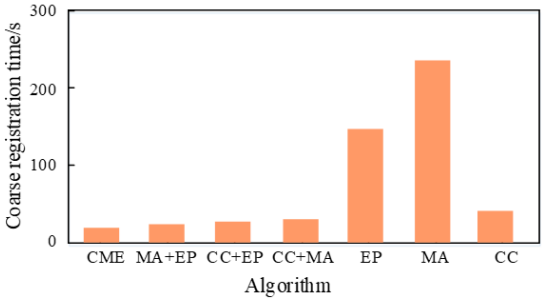

(c) Coarse Registration Time Consumption

Fig. 4.2: Coarse registration results on the ground of Bunny model

Figure 4.2 is a comparison of feature point registration on the ground of the Bunny model; Figure 4.2a shows that MA has the highest number of feature points at 24976, while CME has the lowest number of feature points at 2146. Figure 4.2b shows that the coarse registration error of CME is 0.925 * 10-6 m, which is the smallest among several methods. EP has the largest coarse registration error, with a value of 1.905 * 10-6 m. Figure 4.2c shows that MA has the longest coarse registration time, reaching 228 seconds, while CME has only 19 seconds for coarse registration. In summary, it has been proven that CME has the best registration effect, and the registration effect of the pairwise combination method is better than that of a single method, indicating that the more feature constraints there are, the more advantageous the registration is.

The proposed algorithm is compared with other algorithms under different Gauss white noise, RICP algorithm, NICP algorithm, MR-KICP algorithm and classical ICP algorithm, and the comparison results are shown in Table 4.1. This table shows that compared to the RICP algorithm, the proposed algorithm has a slight decrease in registration error when matching point clouds with 25dB and 35dB noise; However, due to the RICP algorithm falling into a local optimal solution at 30dB, the registration time is extremely short. Compared to the NICP algorithm, the proposed algorithm has a slight decrease in registration accuracy for noise point clouds of 25dB and 35dB; For the 30dB noise point cloud, it decreased by one order of magnitude, and as the noise increased, the efficiency of the algorithm proposed in the study increased by an average of 10.1%; Compared to the MR-KICP algorithm, the proposed algorithm has a longer registration time but smaller registration error. The registration time of the classic ICP algorithm is extremely short, as it falls into a local optimal solution, resulting in significant registration errors.

Table 4.2 is the data obtained by scanning the water bottle (Bottle, 21469) data and the solid 3D scanning of a Chinese guardian lions' statue (Lion, 53841) from different perspectives, and compares the registration effect of the physical data. This table shows that for Bottom point cloud data with smaller points, the proposed

Table 4.1: Point cloud registration results of Bunny model

Algorithm	Registration times/s			Registration error/ (10-4) mm		
	25dB	30dB	35dB	25dB	30dB	35dB
Propose	117.262	88.364	36.393	0.161	0.106	0.058
RICP	114.265	11.966	30.151	0.163	2.309	0.060
NICP	118.097	92.580	56.932	0.164	1.139	0.059
MR-KICP	41.982	38.521	30.337	7.640	6.608	5.308
ICP	0.302	0.380	0.454	64.892	61.980	65.883

Table 4.2: Comparison of physical point cloud registration

Algorithm	Registration times/s		Registration error/ (10-4) mm	
	Bottle	Lion	Bottle	Lion
Propose	7.501	66.332	4.338×10-2	2.293
NICP	9.572	5.045	4.558×10-2	11.876
MR-KICP	25.531	116.423	3.789	357.612
ICP	1.284	10.697	1.212×104	205.213

algorithm reduces registration error by 2 orders of magnitude and registration time by 71.2% compared to MR-KICP; Compared with the NICP method, the registration error has been reduced by 50% and the registration time has been shortened by 21.4%. For Lion point cloud data with larger points, the proposed algorithm reduces registration error by 2 orders of magnitude and registration time by 40.6% compared to MR-KICP. Overall, the algorithm proposed in the study outperforms other algorithms in terms of registration efficiency and accuracy.

4.2. Registration results and analysis. Figure 4.3 shows the comparison results between the original ICP algorithm and the improved ICP algorithm. Figure 4.3a shows that the improved ICP algorithm requires less time to complete accurate registration; Figure 4.3b shows that there is almost no difference in registration error between the two algorithms after registration. Overall, the iteration speeds of the two algorithms are similar, but the horizontal axis indicates that the improved ICP algorithm achieved accurate registration with fewer iterations. So, the improved ICP algorithm reduces the number of iterations while ensuring registration accuracy, thereby improving the efficiency of registration.

To demonstrate the necessity of constructing MSM, this study compared MSM with Normal vector (NV) matrix, Curvature (CU) matrix, point density (PD) matrix, and descriptors composed of pairwise combinations. Figure 4.4 shows the test results under the Dragon model, and Figure 4.4a shows that the registration times of the seven methods are not significantly different. The registration time for MSM is 28.87 seconds, the registration time for CU is the shortest at 27.71 seconds, and the registration time for NV is the longest at 29.05 seconds. Figure 4.4b shows that the registration error of MSM is 0.285 * 10-5 m, which is the smallest among several methods. The coarse registration error of CU is the largest, with a value of 5.256 * 10-5 m. Overall, for more complex Dragon models, using only one sub scale matrix to describe feature points has limited descriptive power, resulting in the highest registration error; After using two sub scale matrices, the registration accuracy has significantly improved. Due to the use of three sub scales in MSM, the registration error is the smallest.

Figure 4.5 shows the test results under the Bunny model; Figure 4.5a shows that the registration time for MSM is 20.22 seconds, the registration time for PD is the shortest at 18.95 seconds, and the registration time for NV+CU is the longest at 20.25 seconds. Figure 4.5b shows that the registration error of MSM is 0.089 * 10-5 m, which is the smallest among several methods. The coarse registration error of PD is the largest, with a value of 0.214 * 10-5 m. Overall, MSM has the best descriptive ability, resulting in matching points that are closest to geometric features.

To verify the higher registration efficiency and accuracy of the proposed registration method, the NDM-KICP algorithm was compared with classical ICP algorithm, LPFH based KICP algorithm (LPFH KICP),

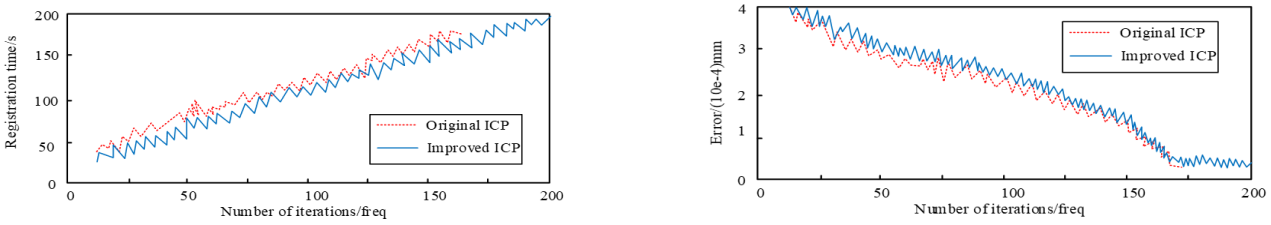

(a) Registration Time Comparison (b) Comparison of Registration Error

Fig. 4.3: ICP algorithm comparison

(a) Coarse Registration Time Comparison (b) Coarse Registration Error

Fig. 4.4: Results of the descriptor experiment on the ground of the Dragon model

NCCP based bidirectional k-tree ICP algorithm (NCCP BKICP), Semidefinite Based Randomized Approach (SBRA), and Sampling Consistency and Non-destructive Testing (SCNT) algorithm, Table 3 is the registration data on the ground of the Bunny model. Table 3 shows that compared to the LPFH-KICP algorithm, the NDM-KICP algorithm has an average reduction of 46.2% in relative rotation error and an average reduction of 30.3% in registration time. Compared to the NCCP-BKICP algorithm, the average relative rotation error is reduced by 44.5%, and the registration time is shortened by 60.2% on average. Compared to the SBRA algorithm, the relative rotation error is reduced by an average of 1-2 orders of magnitude, and the registration time is shortened by an average of 62.7%. Compared to the SCNT algorithm, the average relative rotation error is reduced by 1-2 orders of magnitude, and the registration time is shortened by 93.3% on average.

Table 4.4 is the registration data on the ground of the Dragon model. Table 4 shows that compared to the LPFH-KICP algorithm, the NDM-KICP algorithm has an average reduction of 11.3% in relative rotation error and an average reduction of 12.6% in registration time. Compared to the NCCP-BKICP algorithm, the relative rotation error has been reduced by an average of 16.1%, and the registration time has been shortened by an average of 24.9%. Compared to the SBRA algorithm, the average relative rotation error is reduced by 33.2%, and the registration time is shortened by 24.7% on average. Compared to the SCNT algorithm, the average relative rotation error is reduced by 2-3 orders of magnitude, and the registration time is shortened by 85.5% on average.

5. Conclusion. In response to the low level of automation and poor robustness of DS parameter models, this study studied the application characteristics of DS, and then introduced the ICP algorithm and MSM descriptor to improve the point cloud registration algorithm. A method for constructing DS parameter models

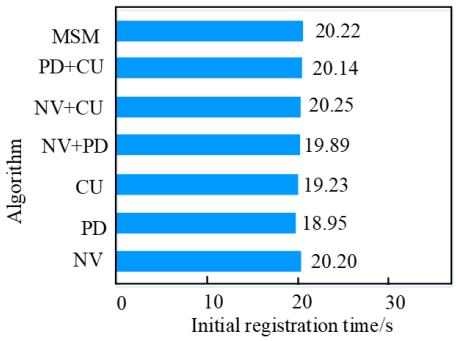

(a) Coarse Registration Time Comparision

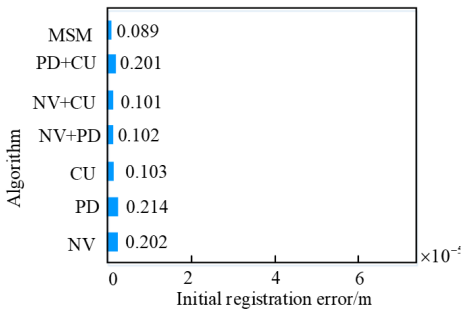

(b) Coarse Registration Error

Fig. 4.5: Results of the descriptor experiment on the ground of the Bunny model

Table 4.3: Registration results of Bunny model

Index	Algorithm	Eliminate point cloud ratio (number of point clouds)			
		5% (34139)	10% (32360)	15% (30548)	20% (28765)
Relative rotation error	NDM-KICP	1.666×10-4	9.192×10-4	83641×10-4	7.265×10-4
	SCNT	2.105×10-2	8.164×10-3	2.324×10-2	2.740×10-2
	SBRA	3.724×10-2	5.106×10-3	7.104×10-2	3.679×10-2
	NCCP-BKICP	1.670×10-4	9.278×10-4	1.490×10-3	2.146×10-3
	LPFH-KICP	3.736×10-4	0.998×10-3	1.416×10-3	2.146×10-3
	ICP	1.476	1.497	1.490	1.492
Registration time	NDM-KICP	15.800	16.352	14.886	13.719
	SCNT	195.084	204.040	250.179	201.8964
	SBRA	42.016	40.846	38.964	38.842
	NCCP-BKICP	36.870	35.996	39.375	37.848
	LPFH-KICP	22.075	22.227	21.748	21.297
	ICP	1.985	1.682	1.739	1.703

Table 4.4: Registration results of Dragon model

		Gaussian white noise ratio			
Index	Algorithm	0.1 $\bar{r}$	0.2 $\bar{r}$	0.3 $\bar{r}$	0.5 $\bar{r}$
Relative rotation error	NDM-KICP	1.305×10-5	4.00910-5	2.19910-5	1.126×10-4
	SCNT	1.769×10-2	1.731×10-2	1.264×10-2	3.492×10-2
	SBRA	1.958×10-5	4.689×10-5	5.475×10-5	1.593×10-4
	NCCP-BKICP	1.308×10-5	4.551×10-5	2.542×10-5	1.397×10-4
	LPFH-KICP	1.309×10-5	4.817×10-5	3.142×10-5	1.174×10-4
	ICP	1.782	1.784	1.782	1.783
Registration time	NDM-KICP	36.785	37.842	44.685	51.896
	SCNT	300.735	301.984	307.692	305.512
	SBRA	77.669	54.671	59.743	67.115
	NCCP-BKICP	52.846	54.183	60.268	62.439
	LPFH-KICP	44.786	45.816	49.558	53.371
	ICP	4.645	4.679	4.762	5.413

on the ground of the improved point cloud registration algorithm was proposed. The results show that under the Bunny model, the number of feature points in CME is only 2146, and the coarse registration error is 0.925 * 10-6 m; As the noise increases, the efficiency of the algorithm proposed in the study increases by an average of 10.1%; The registration time of MSM is 20.22 seconds, and the registration error of MSM is 0.089 * 10-5 meters; Compared to the LPFH-KICP algorithm, the NDM-KICP algorithm has an average reduction of 46.2% in relative rotation error and 30.3% in registration time. Compared to the NCCP-BKICP algorithm, the NDM-KICP algorithm has an average reduction of 44.5% in relative rotation error and 60.2% in registration time. In the Dragon model, the number of feature points in CME is 2235, and the coarse registration time is only 26 seconds; The registration time of MSM is 28.87s, and the registration error is 0.285 * 10-5m; Compared to the LPFH-KICP algorithm, the NDM-KICP algorithm has an average reduction of 11.3% in relative rotation error and 12.6% in registration time. Compared to the NCCP-BKICP algorithm, the NDM-KICP algorithm has an average reduction of 16.1% in relative rotation error and 24.9% in registration time. The digital sculpture parameter model construction method based on improved point cloud registration algorithm proposed in this paper has achieved good results, but some work still needs to be further improved in practical engineering applications. Almost all the existing sculpture modeling methods assume that the background plane of the sculpture is an ideal plane. In the future, it is necessary to study the digital sculpture modeling methods with curved surface or non-convex plane as the background plane. It is also possible to explore a digital sculpture modeling method that can produce optical illusion through light changes, shadow effects or forced perspective, so as to better meet the needs of practical applications.

Fundings. The research is supported by: 2021 basic scientific research business cost research project of Heilongjiang Provincial Colleges and universities, Project No. 2021GJ11; 2022 New Liberal Arts Research and Practice Project, Exploration and Practice of New Liberal Arts Plastic arts Talents' Creative Innovation and Entrepreneurship Cultivation, Project No. XGK2022307.

REFERENCES

[1] Zhang, X., Wang, J., Xiao, J. & Lu, G. Rapid Prototype Design of the Kinetic Sculpture Based on Sketches and Skeletons. *Journal Of Industrial And Intelligent Information*. **8**, 21-26 (2020)

[2] Saeed, M., Ahmad, M. & Rahman, A. Refined Pythagorean Fuzzy Sets: Properties, Set-Theoretic Operations and Axiomatic Results. *Journal Of Computational And Cognitive Engineering*. **2**, 10-16 (2022)

[3] Choudhuri, S., Adeniye, S. & Sen, A. Distribution Alignment Using Complement Entropy Objective and Adaptive Consensus-Based Label Refinement for Partial Domain Adaptation//Artificial Intelligence and Applications. 2023. (0)

[4] Oslund, S., Washington, C. & So, A. Multiview Robust Adversarial Stickers for Arbitrary Objects in the Physical World. *Journal Of Computational And Cognitive Engineering*. **1**, 152-158 (2022)

[5] Wang, X., Cheng, M. & Eaton, J. Fake node attacks on graph convolutional networks. *Journal Of Computational And Cognitive Engineering*. **1**, 165-173 (2022)

[6] Sun, Y., Zhou, D., Wang, J. & Han, H. Lumped Parameter Model for Liquid Sloshing in a Cylindrical Tank Equipped with Multiple Annular Baffles. *Journal Of Structural Engineering*. **147**, 14-27 (2021)

[7] Zhou, S., Liu, X., Hua, Y., Zhou, X. & Yang, S. Adaptive model parameter identification for lithium-ion batteries based on improved coupling hybrid adaptive particle swarm optimization- simulated annealing method. *Journal Of Power Sources*. **482**, 28951-22896 (2021)

[8] Sequeira, S., Bennion, K., Cousineau, J., Validation, N. & Investigations, P. of an Internal Permanent Magnet Motor Using a Lumped Parameter Thermal Model. *Journal Of Electronic Packaging: Transactions Of The ASME*. **144**, 114-123 (2022)

[9] Qin, Z., Wang, C., Peng, Y. & CasViGE, X. Learning robust point cloud registration with cascaded visual-geometric encoding[J]. *Omputer Aided Geometric Design*. **104**, 217-230 (2023)

[10] Zhang, Y., Zhang, C. & Wang, W. Portrait Relief Modeling from a Single Image. *IEEE Transactions On Visualization And Computer Graphics*. **26**, 2659-2670 (2020)

[11] Edward, E., Anikó, E. & And, U. and Shapes to Automatically Form Diverse Digital Sculptures. *SN Computer Science*. **3**, 505-523 (2022)

[12] Zhou, J., Chen, X. & Xu, Y. Automatic Generation of Vivid LEGO Architectural Sculptures. *Computer Graphics Forum*. **38**, 31-42 (2019)

[13] Liu, W., Zhang, L., Zhang, X. & Han, L. Snow Sculpture Reconstruction Based on Structured-Light 3D Vision Measurement. *Applied Sciences*. **11**, 3324-3340 (2021)

[14] Ramazan, A., Erol, S. & Erol, B. An Experimental Study of a New Key point Matching Algorithm for Automatic Point Cloud Registration. *ISPRS International Journal Of Geo-Information*. **10**, 204-232 (2021)

[15] Lanteri, L., Agresti, G. & Pelosi, C. New Practical Approach for 3D Documentation in Ultraviolet Fluorescence and Infrared Reflectography of Polychromatic Sculptures as Fundamental Step in Restoration. *Heritage*. **2**, 207-214 (2019)

[16] Long, X., Chen, Y. & Zhou, J. Development of AR Experiment on Electric-Thermal Effect by Open Framework with Simulation-Based Asset and User-Defined Input//Artificial Intelligence and Applications. 2023. (0)
[17] Islam, A., Othman, F. & Sakib, N. Prevention of Shoulder-Surfing Attack Using Shifting Condition with the Digraph Substitution Rules//Artificial Intelligence and Applications. 2023. (0)
[18] Dornelas, R. & Lima, D. Correlation Filters in Machine Learning Algorithms to Select De-mographic and Individual Features for Autism Spectrum Disorder Diagnosis. *Journal Of Data Science And Intelligent Systems*. **3**, 7-9 (2023)
[19] Wang, J., Yue, K. & Duan, L. and Techniques for Domain Relation Extraction: A Survey. *Journal Of Data Science And Intelligent Systems*. **3**, 16-25 (2023)
[20] Deng, Y., Li, Z. & Chen, J. Interdisciplinary Trends in the Reintegration of Organisms with Perc-eptron Units. Journal of Data Science and Intelligent Systems. *Journal Of Data Science And Intell-igent Systems*. **3**, 44-49 (2023)

Edited by: Zhengyi Chai
Special issue on: Data-Driven Optimization Algorithms for Sustainable and Smart City
Received: Nov 9, 2023
Accepted: Jan 8, 2024